An energetic view on the geographical dependence of the fast aerosol radiative effects on precipitation

Guy Dagan[1], Philip Stier[1] and Duncan Watson-Parris[1]

[1] Atmospheric, Oceanic and Planetary Physics, Department of Physics, University of Oxford, UK

E-mail: guy.dagan@physics.ox.ac.uk

Abstract

By interacting with radiation, aerosols perturb the Earth's energy budget and thus the global precipitation amount. It was previously shown that aerosols lead to a reduction in the global-mean precipitation amount. We have further demonstrated in aqua-planet simulations that the local response to absorbing aerosols differs between the tropics and the extra-tropics. In this study we incorporate an energy budget perspective to further examine the latitudinal dependence of the effect of aerosol-radiation interaction on precipitation in idealized global simulations. We demonstrate that the transition between a positive local precipitation response in the tropics and a negative local precipitation response in the extra-tropics occurs at relatively low latitudes (~10°), indicating a transition between the deep-tropics (in which the Coriolis force is low, hence direct thermally-driven circulation, and associated divergence/convergence of energy/moisture, can form as a result of the diabatic-heating) and their surroundings. In addition, we gradually increase the level of complexity of the simulations and demonstrate that, in the case of absorbing aerosols, the effect of land is to counteract some of the response both inside and outside the deep-tropics due to the reduction in surface latent-heat flux that opposes the diabatic-heating. The effect of scattering aerosols is also examined and demonstrate a decrease in precipitation over land in both the tropics and extra-tropics and no effect over the ocean. Finally, we examine these results in a more realistic set-up and demonstrate that although the physical mechanisms still operate, they are unlikely to be significant enough to be discerned from natural-variability.

Introduction

Aerosol-radiation interactions are known to drive a slowdown of the hydrological cycle (Ramanathan et al., 2001) due to a reduction in the amount of solar radiation reaching the surface and consequently a reduction in surface fluxes. In addition, absorbing aerosols (such as black carbon) lead to a reduction in the global-mean precipitation due to energy budget conservation. Namely, the atmospheric diabetic-heating due to absorbing aerosol is balanced, in the global mean, by a reduction in latent heating by precipitation (Dagan et al., 2019a; Samset et al., 2016). However, previously it was shown that the local precipitation response to an aerosol perturbation in the tropics is the opposite of the global mean response and of the extra-tropical response (Dagan et al., 2019a). That is to say that the same idealized aerosol perturbation was shown to decrease precipitation in the extra-tropics and increase precipitation in the tropics. This contrasting response can be explained by the different ability of the atmosphere to diverge excess dry static-energy in the tropics and extra-tropics (Sobel et al., 2001). In the tropics an atmospheric diabatic-heating (e.g. due to absorbing aerosols) leads to a very efficient distribution of the excess energy for large scales (Gill, 1980; Matsuno, 1966), a large-scale direct thermally-driven circulation (Roeckner et al., 2006) and thus to a large increase in precipitation. In contrast, in the extra-tropics, excess energy from aerosol diabatic-heating is constrained due to the effect of the Coriolis force, causing the precipitation to decrease (to maintain energy balance Dagan et al., 2019a).

Here we examine the aerosol effect on precipitation from a regional energy budget perspective (Dagan et al., 2020; Dagan et al., 2019a; Hodnebrog et al., 2016; Liu et al., 2018; Muller & O'Gorman, 2011; Myhre et al., 2017; Myhre et al., 2018; Richardson et al., 2018; Samset et al., 2016). According to this perspective, any aerosol-driven changes in radiation fluxes must be balanced, on long time scales, by changes in precipitation, sensible heat flux or by divergence of dry static energy.

The long-time average total column atmospheric energy budget can be described as follows:

$$LP + Q_R + Q_{SH} = \mathrm{div}(s) \qquad (1)$$

Where LP is the latent heat due to precipitation, Q_{SH} is the surface sensible heat flux, Q_R is the atmospheric radiative heating, and div(s) is the divergence of dry static energy - which will become negligible on sufficiently large spatial scales (Jakob et al., 2019). Equation 1 provides information on the time mean precipitation rate and not on the distribution of rainfall intensities, which may change under aerosol forcing as well (e.g. (Zhao et al., 2019)).

Local changes in precipitation due to an aerosol perturbation could be caused by microphysical feedbacks (Khain, 2009; Levin & Cotton, 2009), by local changes to the energy budget (radiation fluxes or surface sensible heat flux changes) or by changes to the general circulation of the atmosphere, caused by the inhomogeneous aerosol radiative effect (Chemke & Dagan, 2018). For example, asymmetry in aerosol radiative effect between the two hemispheres were shown to leads to cross-equatorial energy flux a thus to a shift in the intertropical convergence zone (Allen et al., 2015; Rotstayn & Lohmann, 2002; Voigt et al., 2017; Wang, 2015). Aerosols-driven changes to the extra-tropical atmospheric circulation may also lead to changes to the spatial distribution of precipitation (Allen & Sherwood, 2011; Chemke & Dagan, 2018; Ming et al., 2011).

In this study we use General Circulation Model (GCM) simulations in two configurations (with and without land) to study the fast precipitation response (under prescribed sea surface temperature - SST (Bony et al., 2013; Myhre et al., 2018; Richardson et al., 2018)) to idealized and more realistic aerosol perturbation at different locations. This set of simulations enable us to expand the analysis presented in Dagan et al. (2019a) in which the differences between the tropics and extra-tropics were demonstrated using idealized global simulations (using aqua-planet configuration and idealized, large aerosol perturbations). This paper addresses the following questions: 1) What latitude does the local precipitation response to absorbing aerosol perturbations shifts from positive in the tropics to negative in the extra-tropics? 2) What is the effect of land on the above-mentioned response, and 3) What is the effect of the spatial structure and magnitude of aerosol perturbation when going from highly idealised to more realistic simulations?

Methodology

Model

The ICON (icosahedral nonhydrostatic) atmospheric GCM (Crueger et al., 2018; Giorgetta et al., 2018; Zängl et al., 2015) is used in aqua-planet and AMIP (Atmospheric Model Inter-comparison Project (Gates, 1992)) configurations. For both the aqua-planet and AMIP simulations we use a grid with an effective resolution of 157.8 km [R2B04 (Zängl et al., 2015)] and 47 vertical levels.

The representation of the radiative effect of aerosols is through MACv2-SP [Max Planck Institute Aerosol Climatology version 2, Simple Plume (Kinne et al., 2013; Stevens et al., 2017)]. This relatively simple aerosol model prescribes the anthropogenic aerosol optical depth (AOD) and its radiative properties (the single scattering albedo – SSA, and the asymmetry parameter), as functions of time, geographical location and wavelength. The aerosol characteristics in the MACv2-SP are based on long term observations (Kinne et al., 2013; Stevens et al., 2017). There is no coupling between aerosol and cloud microphysics, i.e. only the aerosol radiative effect is considered. For more details about MACv2-SP the reader is referred to Stevens et al. (2017).

Aqua-planet simulations

Nine simulations are conducted in the aqua-planet configuration– one reference simulation with no aerosol forcing, and 8 simulations with different aerosol plume centres between 0^o and 70^o in continues increments of 10^o. As in Dagan et al. (2019a), the reference simulation is run for 10 years (to account for natural variability), while each of the perturbed simulations are run for 4 years and reach a stationary-state.

In the aqua-planet simulations, we use an idealized and strong aerosol perturbation with a simple Gaussian spatial distribution around the plume centre (Dagan et al., 2019a). The radius of the tropical plume is set to 10° in both the north-south and east-west directions. As in Dagan et al. (2019a), the AOD magnitude at the centre of the tropical plume is equal to 2.4, which is the global sum of all plumes in the default MACv2-SP setup, i.e. a very strong local perturbation. We correct for the different width of a degree longitude and for the differing amounts of incoming solar radiation between the different simulations with the different aerosol plume locations. We do that by increasing the plume zonal dimensions and the AOD magnitude at the centre of the plume by a factor of $1/\cos(lat)$, where *lat* is the latitude of the plume centre. Hence, for each simulation the global mean perturbation is similar regardless of the plume location. The SSA in this case is set to 0.8.

AMIP simulations

In the AMIP simulations, each simulation is run either for 10 (idealized perturbations) or 30 (more realistic perturbations) years. For the idealized perturbation simulations, we use similar plume characteristics as in the aqua-planet simulations (radius of 10^o and AOD=2.4). The plume centre is located either at the tropics (0^o – for three different longitudes, two over land and one over the ocean) or at the extra-tropics (40^o – for three different longitudes, two over land and one over the ocean, Fig. 1). For each plume location two different SSA of 0.8 and 1 are used.

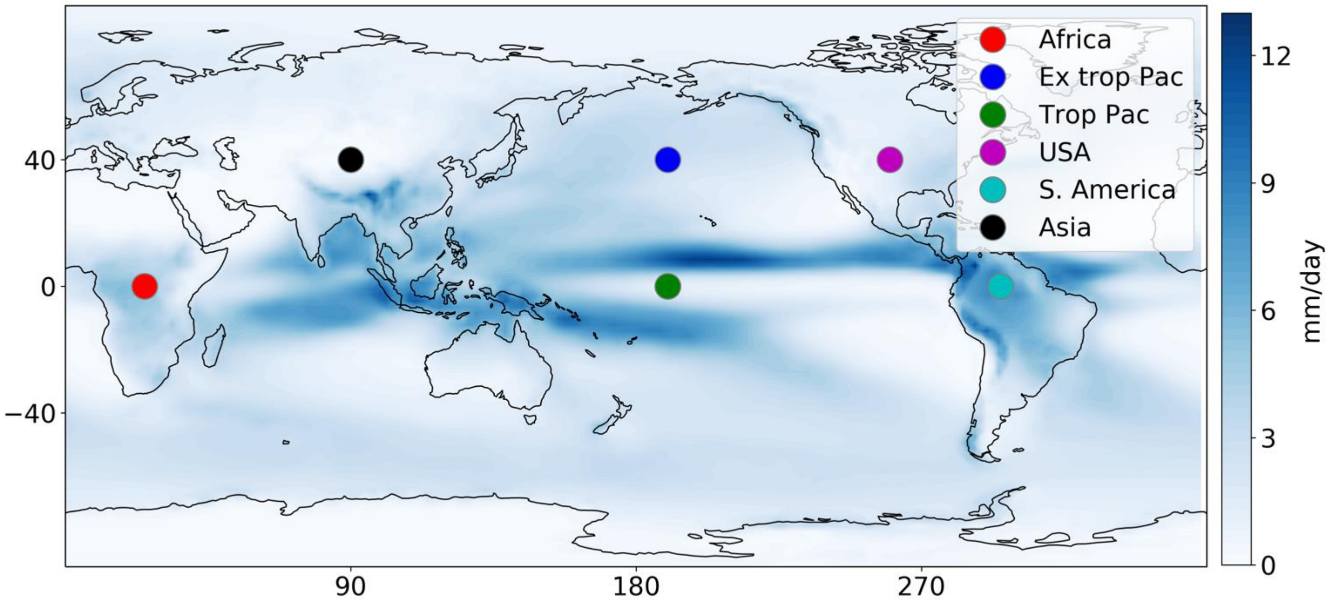

Figure 1. The locations of the aerosol plume centres for the AMIP ICON simulations forced with the MACv2-SP aerosol plume model. The background represents the time-average surface precipitation over the 30 years simulation in the reference case (no anthropogenic aerosols).

For the more realistic perturbations we use the default MACv2-SP setup, either including the entire global distribution of aerosol (Full plume) or specific regional plumes. Each simulation was conducted for 30 years. In the single plume simulations, the AOD in each plume was set to its value at 2005, while for the Full plume simulations the AOD in each plume changed with time according to the MACv2-SP setup for the years 1979-2009.

Results

The latitudinal dependence of the fast aerosol effect on precipitation

To identify the latitude of the transition between the positive local precipitation response due to an absorbing aerosol perturbation in the tropics and the negative local response in the extra-tropics we use the aqua-planet simulations with a stepwise change in the aerosol plume location. Figure 2 presents the atmospheric radiative heating (Q_R) perturbation generated in these simulations, while Fig. 3 presents the relative precipitation response (the absolute precipitation response is presented in Figs. S1-S2, SI). As expected, for all latitudes the presence of absorbing aerosols generates a positive Q_R perturbation. The magnitude of the Q_R perturbation slightly decreases with latitude due to the clouds' response to the Q_R perturbation – i.e. deeper clouds formation in the tropics and hence reduction in the outgoing longwave flux and larger Q_R perturbation compared to the extra-tropics (Dagan et al., 2019a). The local precipitation response to this positive Q_R perturbation is positive in the tropics (0^o and 10^o) and negative in the extra-tropics (30^o and above – see also Fig. 4 presenting the precipitation response at the centre of the aerosol plume as a function of the location of the plume). The simulations in which the aerosol plume centre is located at 10^o and 20^o demonstrates an increase in precipitation at the south part of the plume and a small or even negative response at the north part (Fig. 3). At the plume centre, the precipitation response is slightly positive for the simulation with the plume centre at 10^o and negative for the simulation with the plume centre at 20^o (Fig. 4).

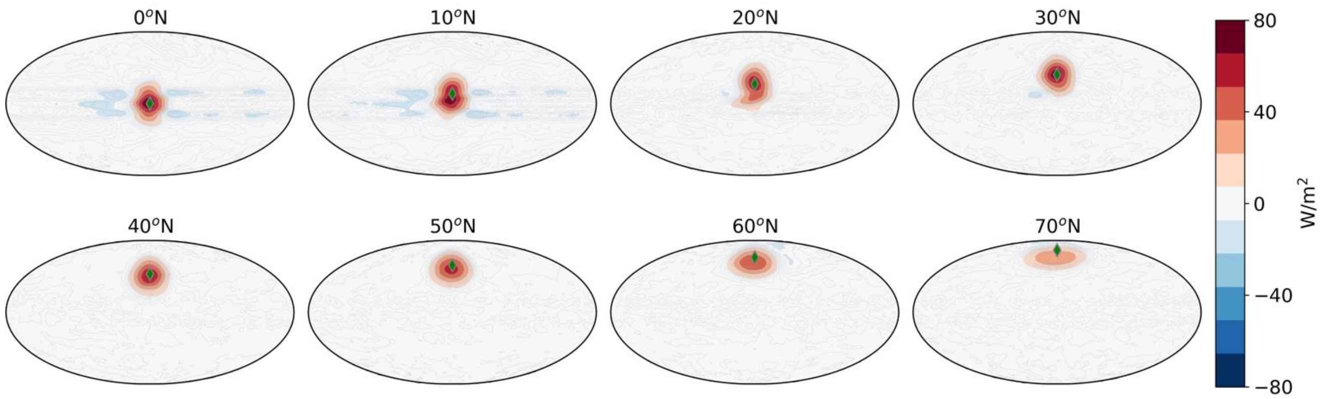

Figure 2. The atmospheric radiative heating (Q_R) perturbation (each simulation minus the reference simulation) in the aqua-planet ICON simulations. For each simulation the aerosol plume centre is indicated in the title and is marked by a green diamond.

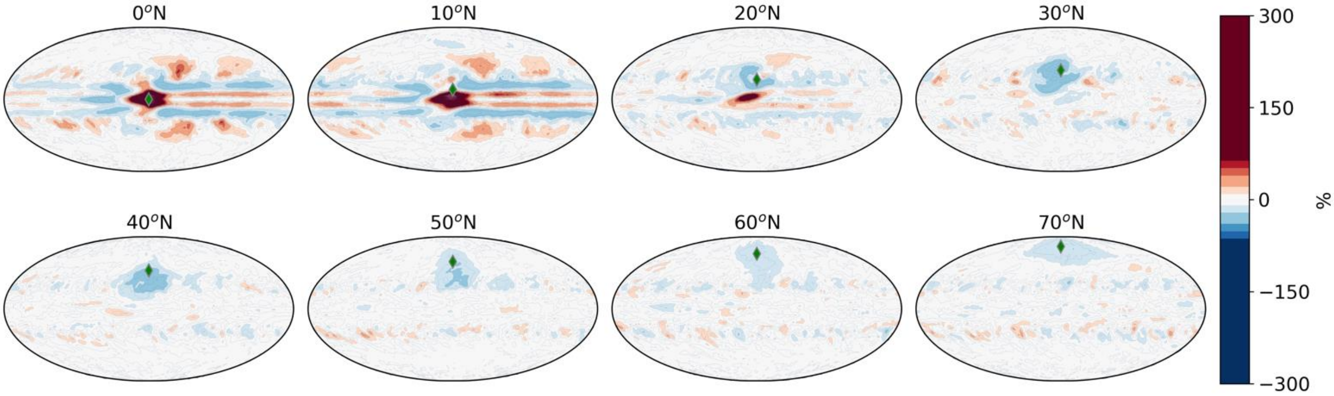

Figure 3. The relative precipitation change (compared to the reference simulation) for the aqua-planet ICON simulations. For each simulation the aerosol plume centre is indicated in the title and is marked by a green diamond.

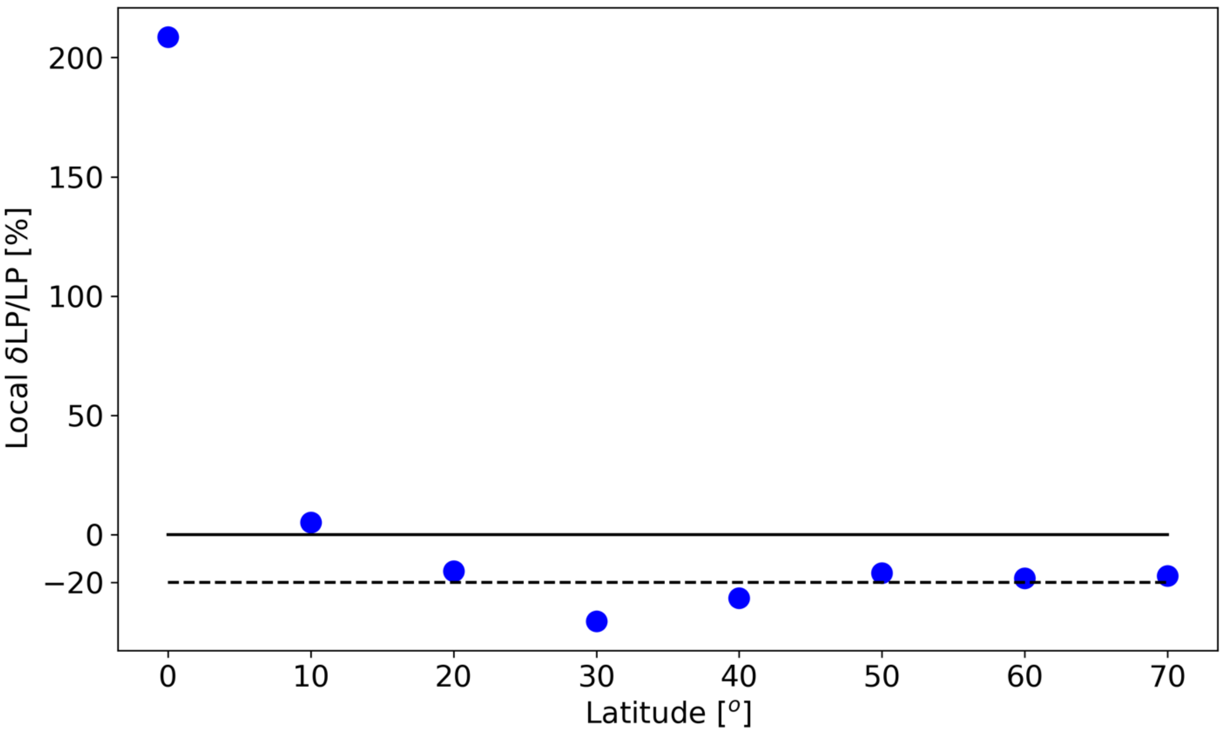

Figure 4. The relative precipitation change (compared to the reference simulation) at the centre of the aerosol plume as a function of the centre latitude location in the aqua-planet ICON simulations. Black solid and dashed horizontal lines mark the 0 and -20% levels, respectively, for reference.

Examining the meridional cross-sections of the precipitation response at the longitude of the plume centre (Fig. 5) demonstrates that the transition between a positive precipitation response at the tropics and a negative response outside the tropics occurs at roughly 10^{o}. This result indicates that the latitude of the transition between the different responses is at fairly low latitudes, and that the positive response occurs only in the deep-tropics where the Coriolis effect is negligible. This result can be understood by the fact that at latitudes higher than 10^{o} the Coriolis force is already sufficient, for example, to generate a tropical cyclone (Gray, 1975), and hence prevent the direct thermally-driven circulation that was shown to be generated in the tropics (Dagan et al., 2019a; Roeckner et al., 2006; Stuecker et al., 2020). At latitudes higher than 10^{o}, geostrophic adjustment of the flow confines the heating perturbations. On the other hand, at latitudes lower than 10^{o}, the mass field adjusts to the diabatic-heating, i.e. mass converges into the heating anomaly, which then generates vertical motion and supports an increase in precipitation.

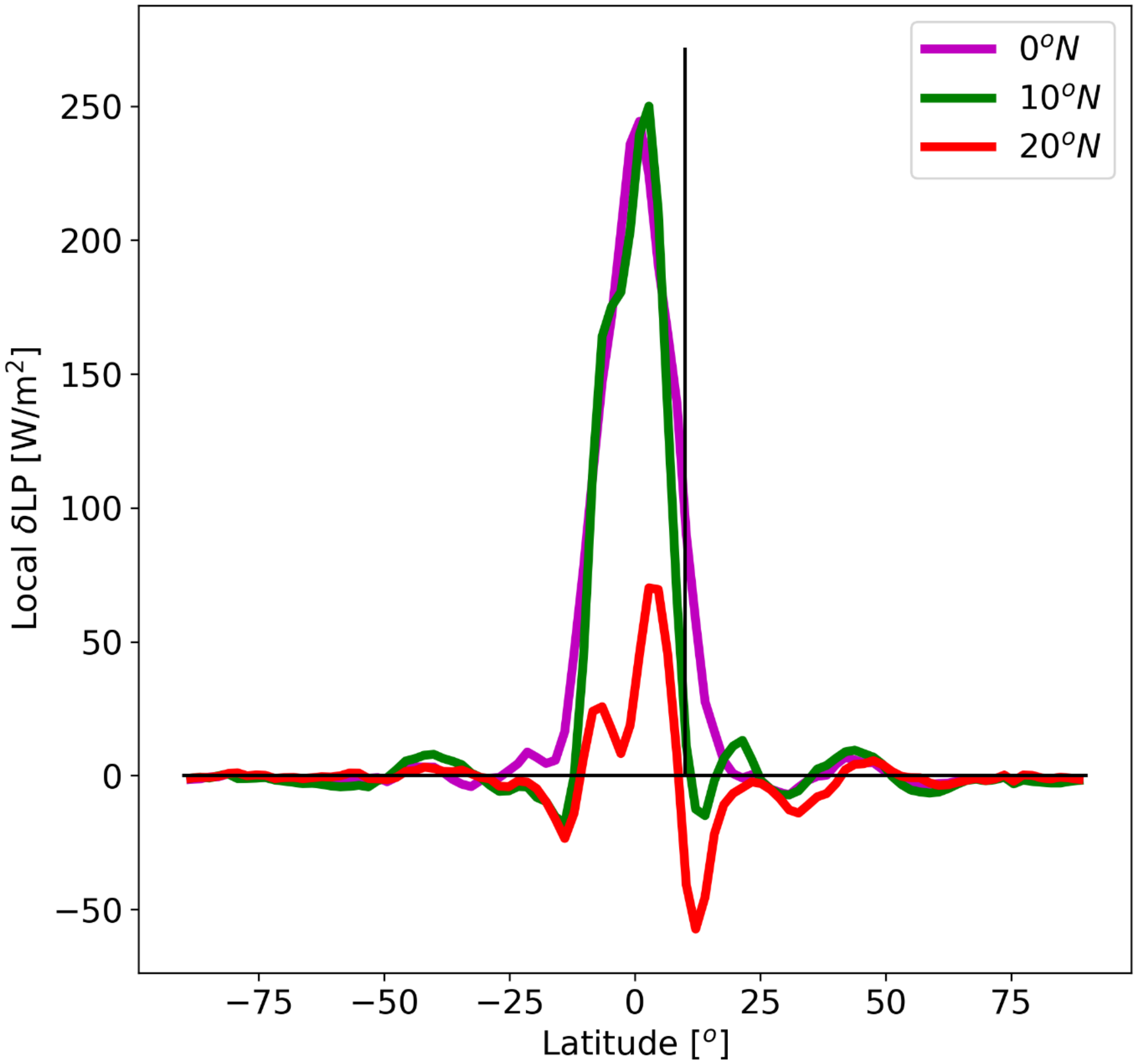

Figure 5. Meridional cross-sections of the precipitation response (compared to the reference simulation) at the longitude of the plume centre for the aqua-planet ICON simulations in which the plume centre is at 0°, 10° N and 20° N. The black vertical line marks a latitude of 10° N.

<u>Fast aerosol effect on precipitation over land and ocean</u>

To investigate the similarities and differences between aerosol radiative effects on precipitation over land and ocean we use the AMIP simulations. In the AMIP configuration the SST is prescribed but the land surface temperature is allowed to react to the surface energy budget. This enable investigation of the fast effect (only over land) of aerosol-driven surface temperature changes (which derive changes in Q_{SH}) on precipitation. As a first step, we force the model with a similar idealized, large aerosol perturbation as in the aqua-planet simulations, in the tropics and extra-tropics, over the ocean or land (Fig. 1). In this case we use either absorbing (SSA=0.8) or scattering (SSA=1) aerosols. Figure 6 presents the Q_R perturbations in these simulations and demonstrates a small perturbation in the case of scattering aerosol and a large and positive perturbation in the case of absorbing aerosols.

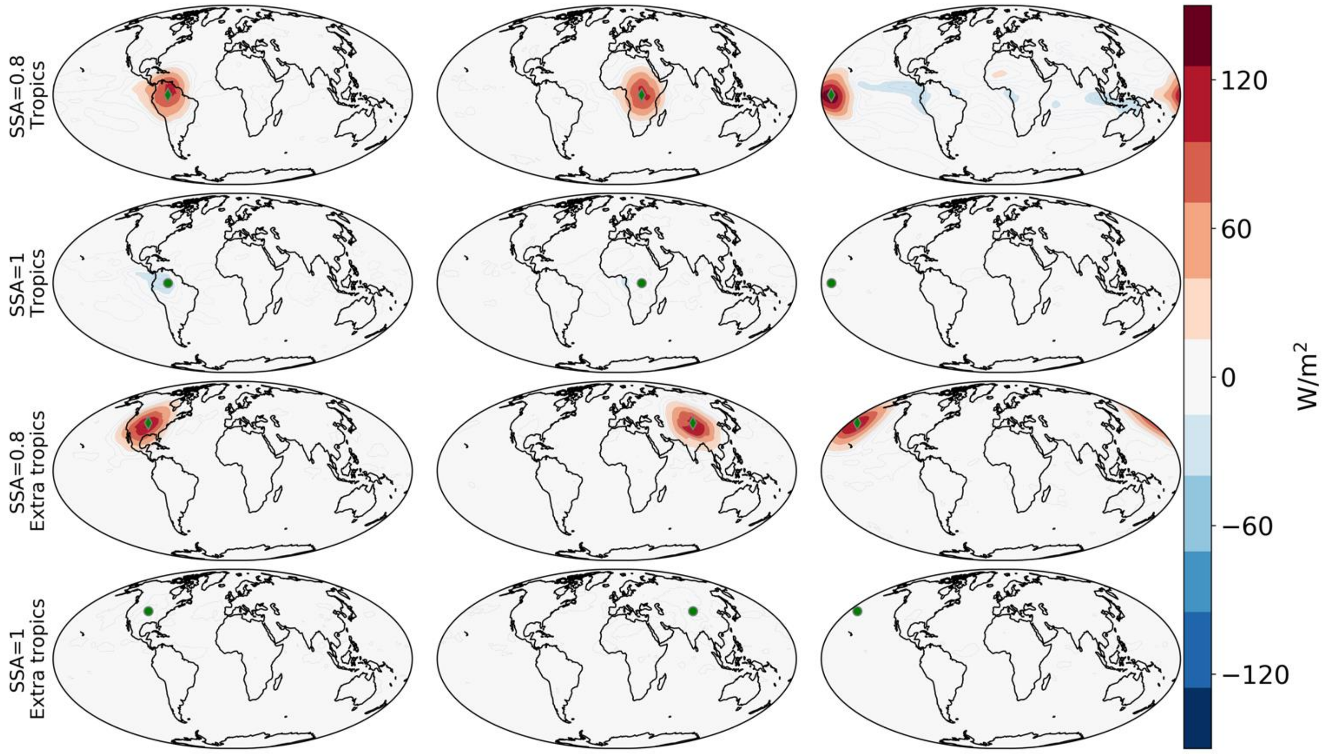

Figure 6. The atmospheric radiative heating (Q_R) perturbation (each simulation minus the reference simulation) in the AMIP ICON simulations forced by idealized aerosol perturbation. For each simulation the aerosol plume centre is marked by a green indicator – circles for scattering aerosol (SSA=1) and diamonds for absorbing aerosols (SSA=0.8).

Figures 7 and 8 present the precipitation and Q_{SH} response to the aerosol perturbations. It demonstrates a decrease in precipitation due to scattering aerosols over land in both the tropics and extra-tropics concomitantly with a reduction in Q_{SH} (over the extra-tropics). On the other hand, over the ocean, in a fixed SST configuration, scattering aerosols have no effect on either the precipitation or Q_{SH}. Like in the case of absorbing aerosols, we note that in the case of scattering aerosols over the tropics the local energy budget is not closed and requires large-scale convergence of energy (the opposite sign as in the case of absorbing aerosols which generate large-scale divergence of energy). This efficient large-scale energy transport is supported in the tropics (Gill, 1980; Matsuno, 1966; Sobel et al., 2001) much more than in the extra-tropics, in which the local energy budget is closer to balance.

Absorbing aerosol perturbation over the ocean, unsurprisingly, generates a similar response as in the aqua-planet configuration (a positive precipitation response in the tropics and a negative response in the extra-tropics, without any effect on Q_{SH}). Over land, as in the aqua-planet case, the precipitation response to absorbing aerosols is negative in the extra-tropics and a negative Q_{SH} response is also seen. This negative Q_{SH} response is caused by a reduction of the solar radiation reaching the surface. Over tropical land, the absorbing aerosol perturbation generates a more complex precipitation response. In the case of absorbing aerosols over South-America, the precipitation response is mostly negative over land and positive over the adjacent oceans. Over Africa the precipitation response is more positive over land (although there are places in which it is negative) and, as in the South-America case, positive and larger over the adjacent oceans. The smaller precipitation response to absorbing aerosol over tropical land (compared to over the ocean) can be understood by the fact that the negative Q_{SH} response (Fig. 8) counteract some of the positive Q_R tendency to generate direct thermally-driven circulation. In addition, we note that the positive precipitation response over the east-tropical Atlantic is accompanied by a negative response over the west-tropical Atlantic. This is due to a zonal overturning circulation which is formed due to the aerosol effect leading to upward motion in the east Atlantic and downward motion in the west (see Figs S3-4, SI). A similar zonal response of a negative precipitation perturbation west of the plume centre (in which there is a positive precipitation response) is seen in the aqua-planet simulations (see Fig. 3, plume centre at 0^{o} and 10^{o}), in the simulations with the absorbing aerosol plume over South-America (showing a decrease in precipitation over the central-tropical Pacific), and over the tropical Pacific (showing a decrease in precipitation over the Maritime Continent region). In the AMIP simulations there is an additional asymmetry introduced by land.

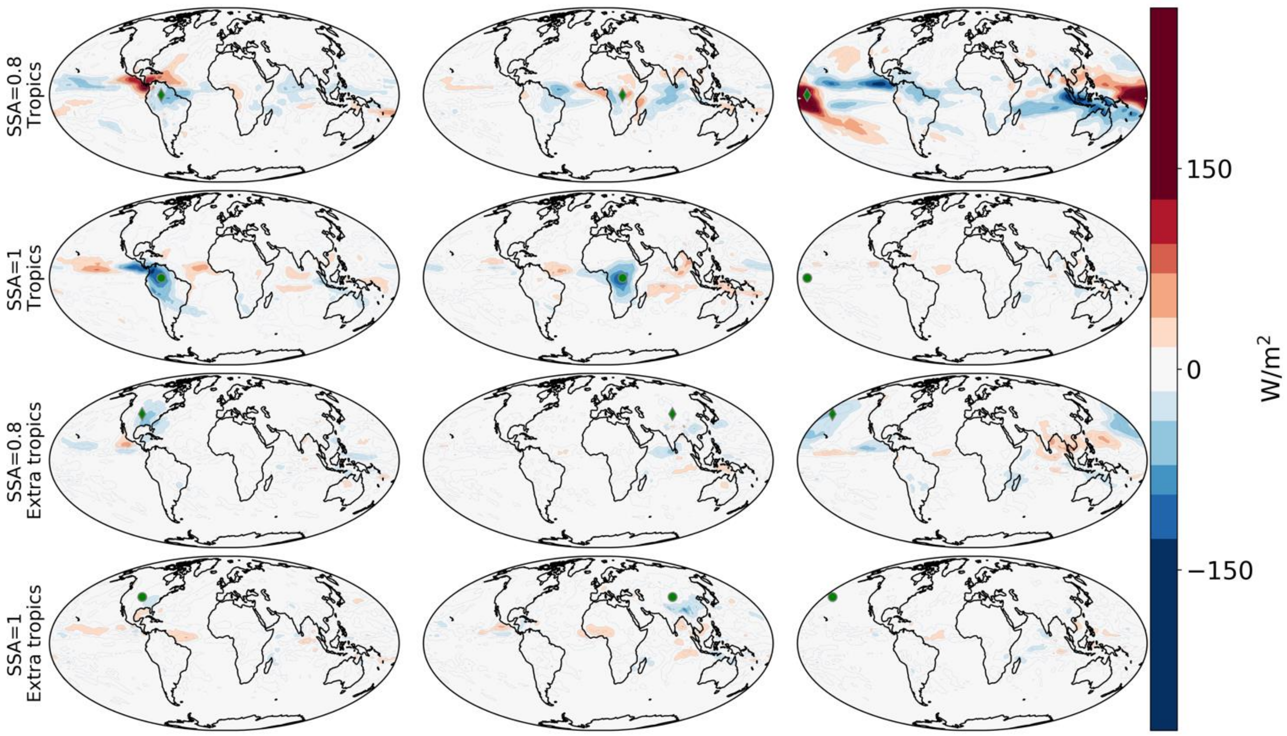

Figure 7. The precipitation latent heating change (compared to the reference simulation) in the AMIP ICON simulations forced by idealized aerosol perturbation. For each simulation the aerosol plume centre is marked by a green indicator – circles for scattering aerosol (SSA=1) and diamonds for absorbing aerosols (SSA=0.8).

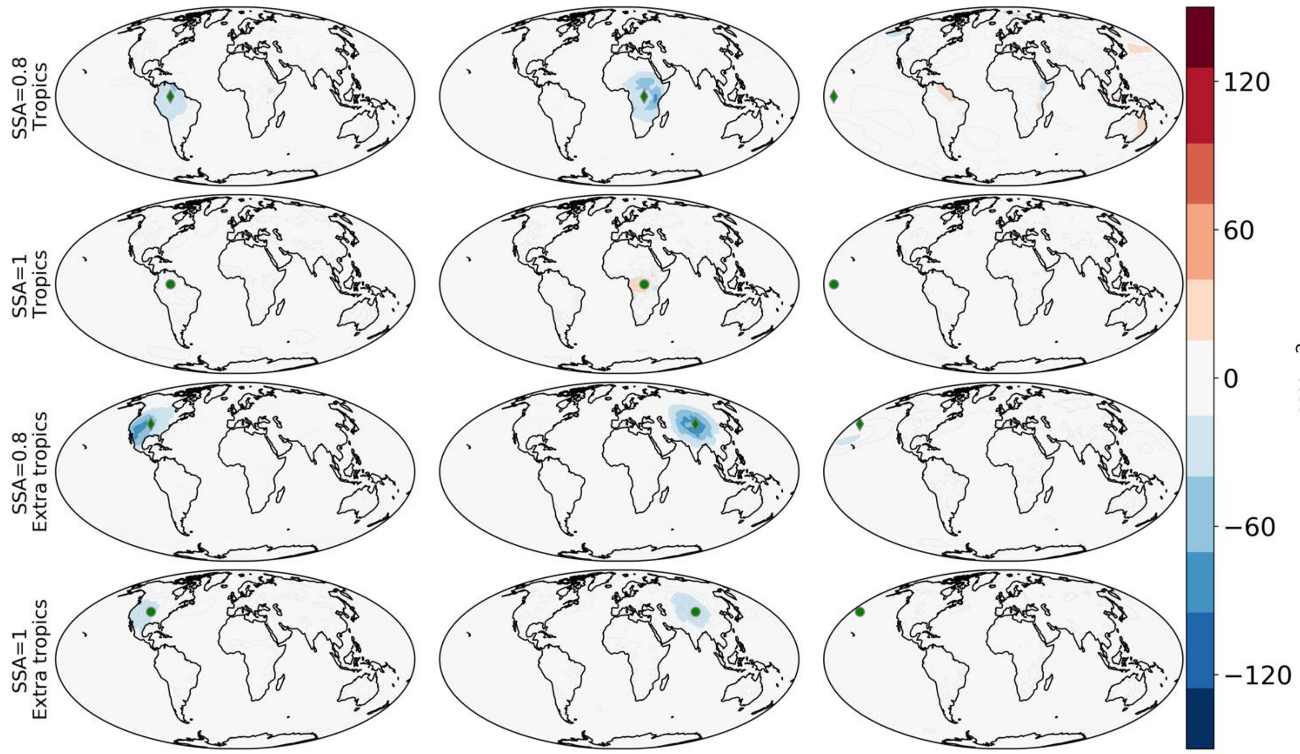

Figure 8. The sensible heat flux (Q_{SH}) change (compared to the reference simulation) in the AMIP ICON simulations forced by idealized aerosol perturbation. For each simulation the aerosol plume centre is marked by a green indicator – circles for scattering aerosol (SSA=1) and diamonds for absorbing aerosols (SSA=0.8).

Figures 9 and 10 present the surface temperature and pressure response to scattering and absorbing aerosol perturbation, respectively, over the extra-tropics (the surface pressure is much less effected by aerosol perturbations over the tropics than over the extra-tropics due to the mass field adjustment). It demonstrates that both scattering and absorbing aerosols cause a reduction in surface temperature over land due to a reduction in surface shortwave radiation. However, a similar negative surface temperature perturbation drives a differing pressure response of an increase in the case of scattering aerosols (Fig. 9) and a slight decrease in the case of absorbing aerosols (Fig. 10). Over the ocean the surface temperature is not allowed to change so the surface pressure does not change much in the case of scattering aerosols (Fig. 9), but decreases significantly in the case of absorbing aerosols (Fig. 10).

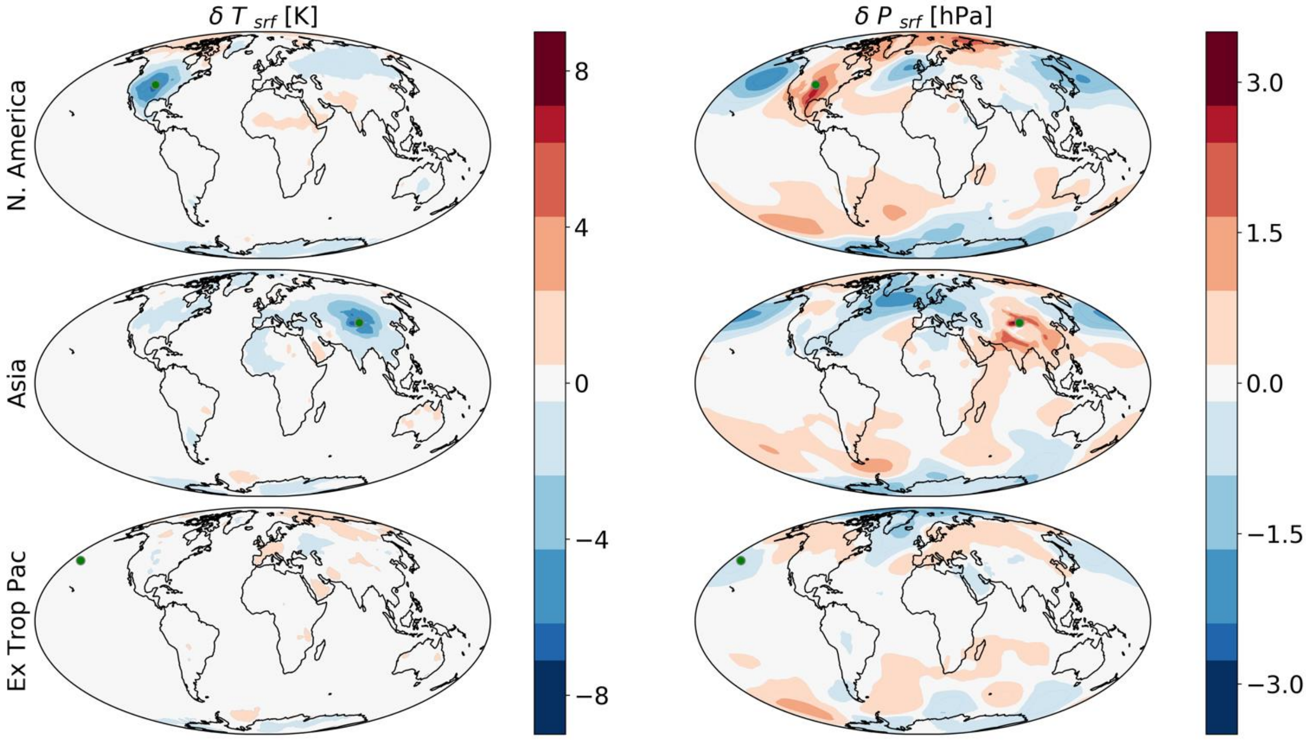

Figure 9. The surface temperature change (δT_{srf} – compared to the reference simulation, left column), and the surface pressure change (δP_{srf} - right column) in the AMIP ICON simulations forced by idealized aerosol perturbation located at the extra-tropics with scattering aerosols (SSA=1). For each simulation the aerosol plume centre is marked by a green circle.

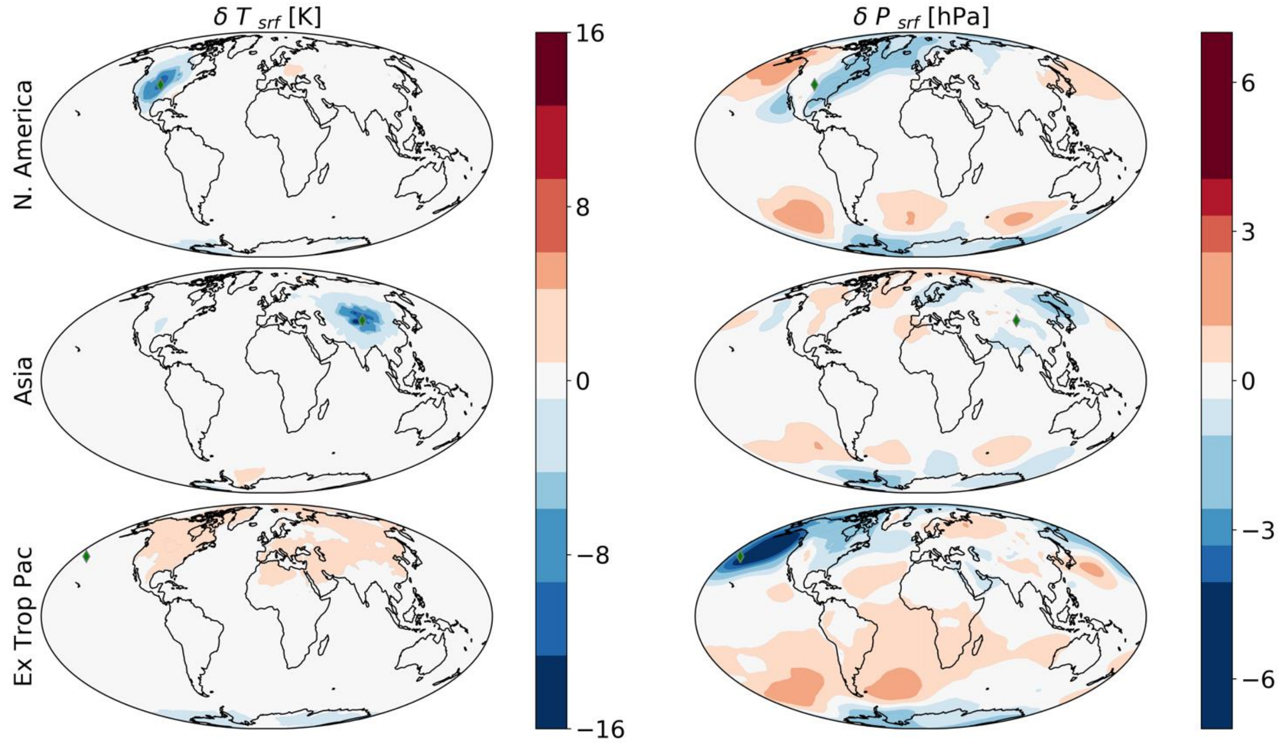

Figure 10. The surface temperature change (δT_{srf} – compared to the reference simulation, left column), and the surface pressure change (δP_{srf} - right column) in the AMIP ICON simulations forced by idealized aerosol perturbation located at the extra-tropics with absorbing aerosols (SSA=0.8). For each simulation the aerosol plume centre is marked by a green diamond.

To better understand these results we examine zonal and meridional cross-sections of the temperature (*T*) response and three components of the wind (*u*, *v* and *ω* for the zonal, meridional and vertical winds, respectively). We do that for the simulations in which the plume is located over North-America, as an example (Figs. 11-12, Figs S3-4, SI present similar cross-section for the simulation in which the aerosol plume is located over Africa as an example of tropical aerosol plume). These results demonstrate that scattering aerosols lead to a cooling of both the surface and the entire troposphere. This cooling of the atmospheric column causes the increase in surface pressure (Fig. 9), which generates an anti-cyclonic circulation around the plume centre (see the response of *v* and *u* in the case of SSA=1 in Figs. 11 and 12, respectively). This anti-cyclonic circulation is accompanied by a positive *ω* perturbation (representing subsidence - Figs. 11-12) and hence also reduction in cloudiness and precipitation (Fig. 7). In the case of absorbing aerosols on the other hand, the temperature response demonstrates a reduction near the surface (due to the reduction in surface shortwave radiation - see also Fig. 10) and an increase above it (due to the direct effect of the absorbing aerosols) this contrasting temperature response with height leads to the small (mostly negative) surface pressure response (Fig. 10). In the extra-tropics, absorbing aerosols generate a weak dynamical response, which mostly reflects a pattern of stationary-waves (Dagan et al., 2019a).

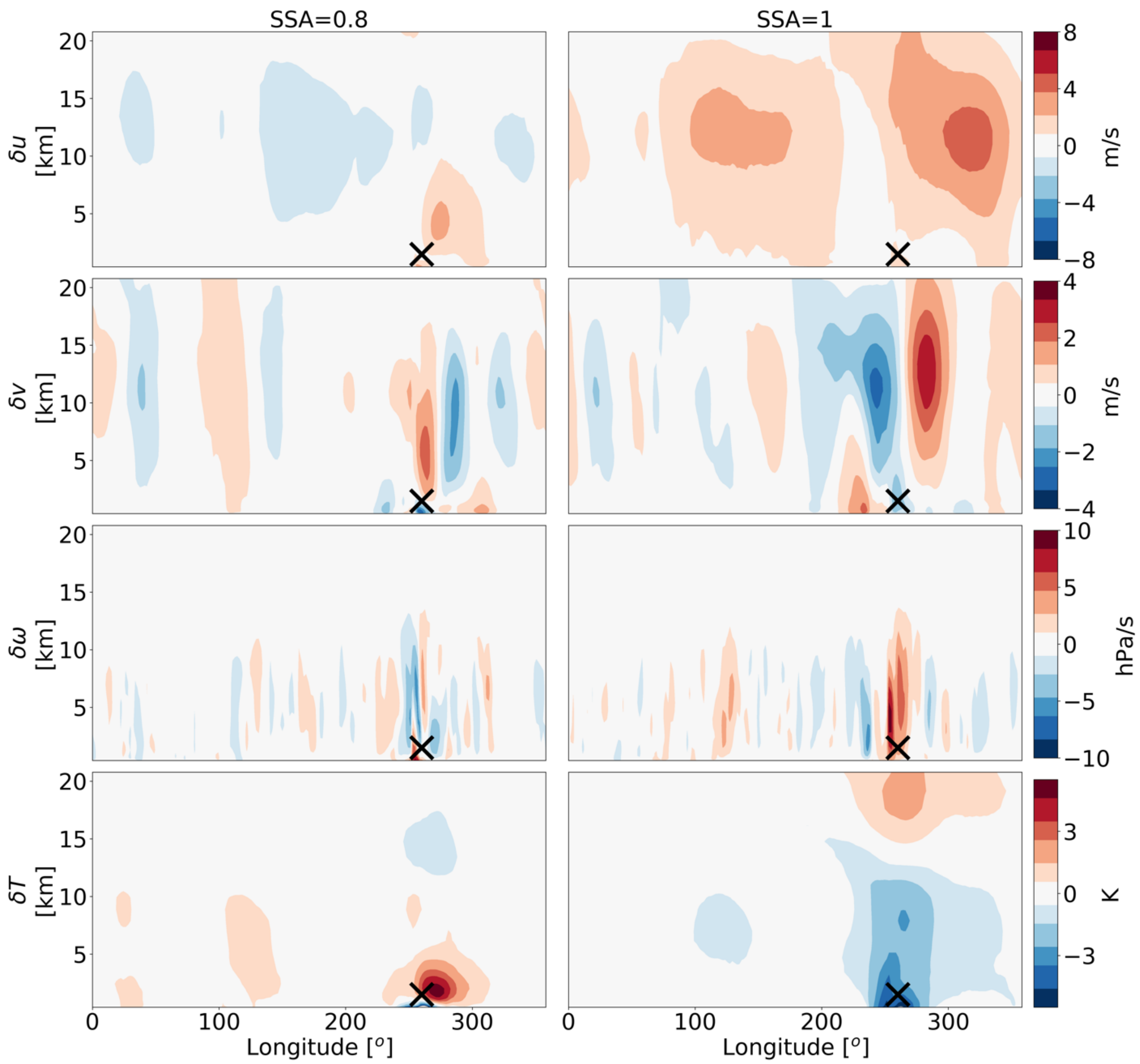

Figure 11. Zonal cross-sections across the latitude of the aerosol plumes' centre (marked by "x") of differences from the reference simulation in eastward winds (δu), northward winds (δv), vertical winds ($\delta \omega$), and temperature (δT). The left column presents the ICON simulation in which the aerosol plume is located over North-America with absorbing aerosols (SSA=0.8), while the right column presents the simulation with the same plume location but with scattering aerosols (SSA=1).

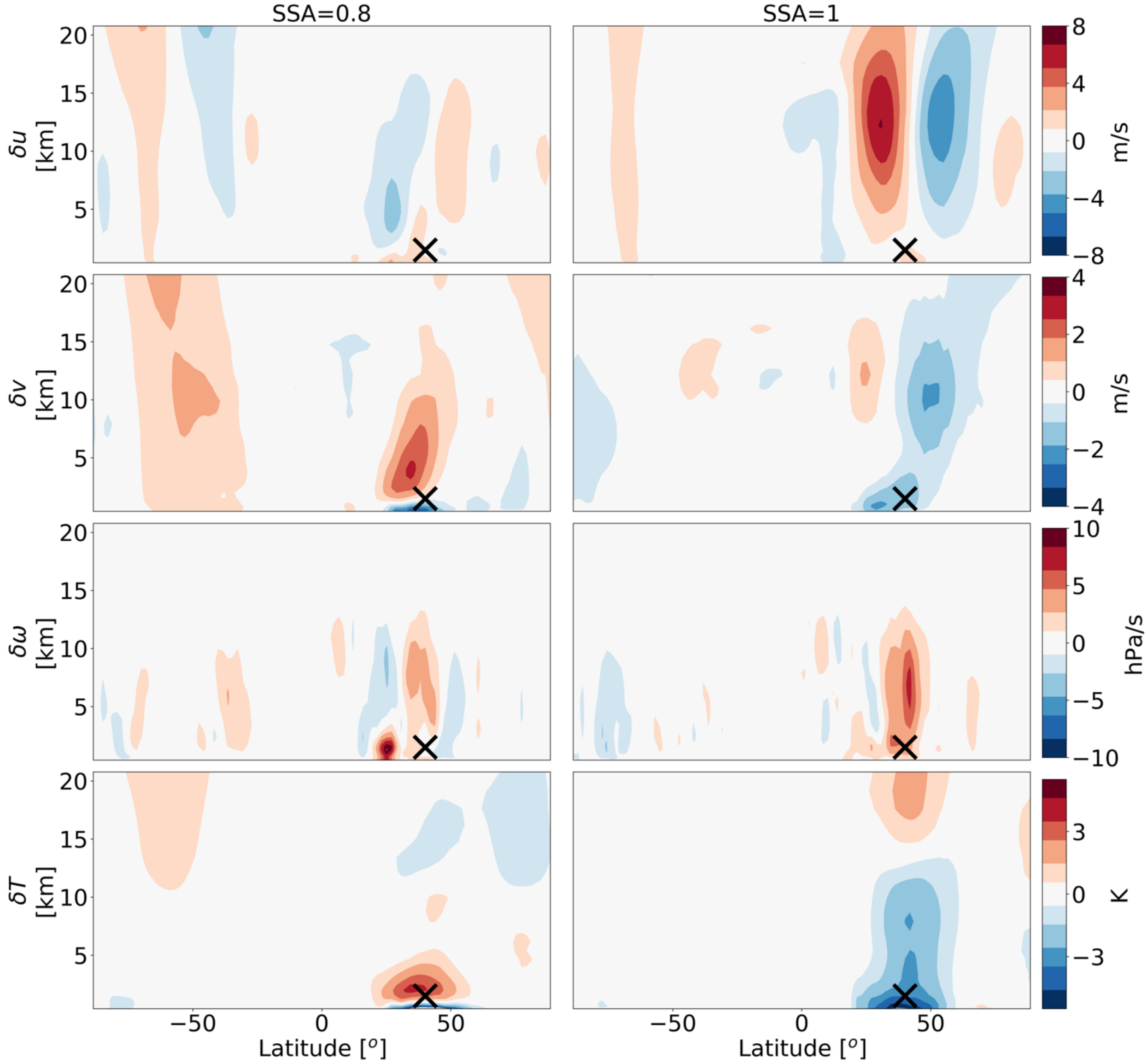

Figure 12. Meridional cross-sections across the longitude of the aerosol plumes' centre (marked by "x") of differences from the reference simulation in eastward winds (δu), northward winds (δv), vertical winds ($\delta\omega$), and temperature (δT). The left column presents the ICON simulation in which the aerosol plume is located over North-America with absorbing aerosols (SSA=0.8), while the right column presents the simulation with the same plume location but with scattering aerosols (SSA=1).

To sum up this section, in the case of absorbing aerosols, the effect of land reduces both the positive fast precipitation response in the tropics and the negative fast response in the extra-tropics due to the larger effect of Q_{SH} (compared to over the ocean), which counteract the diabatic-heating. In the case of scattering aerosols, the absence of any diabatic-heating lead to a reduction in precipitation over tropical and extra-tropical lands due to the reduction in surface shortwave radiation.

Fast aerosol effect on precipitation under more realistic perturbations

So far, we examined the precipitation response to idealized and very strong aerosol perturbations. This is useful for understanding the underlying physics (and a common practice in research of aerosol effect on precipitation, e.g. Myhre et al., 2017). However, one needs to remember that the effect of a more realistic perturbation, even if the same physics applies, may be obscured by natural variability (and also by other external forcings operating at the same time such as green-house gases). In order to examine whether a similar response, as in the idealized perturbations case, can be detected under a more realistic perturbation, we use the default MACv2-SP setup which is based on observed anthropogenic aerosol perturbation. We note that using a non-interactive SST (as in the AMIP configuration) reduces some of the internal-variability of the climate system, hence, these simulations serves as a best case for detectability of the fast aerosol effect on precipitation. As a first step we use idealised, but broadly realistic aerosol plumes in each simulation, representing different geographical locations and different aerosol properties, to examine whether or not the response is consistent with the results described above. The aerosol plumes that we use are: the two African plumes (representing relatively absorbing aerosols mostly over tropical land), the Maritime Continent plume (representing relatively absorbing aerosols mostly over tropical ocean), the two Asian plumes (representing relatively scattering aerosols centred outside the deep-tropics but spending also into the deep-tropics – latitudes lower than 10^o, mostly over land) and the European plume (representing relatively scattering aerosols mostly over extra-tropical land - Table 1).

Table 1. Names followed Stevens et al. (2017), location of centre, AOD (aerosol optical depth) and SSA (single scattering albedo) of the individual plumes used to force the model (the two African and two Asian plumes are used together).

Source region	Latitude	Longitude	Anthropogenic AOD at 550 nm (2005)	SSA at 550 nm
South central Africa	-3.5	16.0	0.372	0.87
North Africa	3.5	22.5	0.211	0.87
Maritime Continent	-1.0	106.0	0.257	0.87
South Asia	23.3	88.0	0.259	0.93
East Asia	30.0	114.0	0.636	0.93
Europe	49.4	20.6	0.148	0.93

Figure 13 presents the Q_R perturbation generated by forcing the model with each plume separately and the precipitation and Q_{SH} response to this perturbation. It demonstrates that, in the tropics, a positive Q_R perturbation due to absorbing aerosols generates a positive precipitation response. This is with agreement with the results from the idealized perturbations above. We note that the precipitation response over the ocean (in the case of the Maritime Continent plume and the adjacent ocean in the African case) is stronger than the response over land (Africa). As was explained above, the smaller precipitation response over land (compared to over the ocean) is due to the reduction in Q_{SH}, which weakens the formation of the thermally-driven circulation. As in the idealized perturbation, the positive precipitation response over the eastern tropical Atlantic, generated by the African plume, drives a negative response over the western tropical Atlantic due to a formation of zonal overturning circulation leading to upward motion in the east Atlantic and downward motion in the west (Figs. S3-4, SI).

In the simulation which is forced by the two Asian plumes, the precipitation increases at the southern part of the plume, over the Indian ocean (reaching all the way to the deep-tropics), while it decreases over the northern part of the plume over east Asia (over land). This, again, is with agreement with the general trend presented above based on the idealized perturbation, of an increase in precipitation in the deep-tropics and a decrease outside the deep-tropics. In addition, we note here again a larger tendency toward a positive response over tropical oceans than over tropical lands due to the role of Q_{SH}. The European plume, which is confined to the extra-tropics, generates a weak Q_R perturbation due to a relatively low AOD and a high SSA. This weak Q_R is accompanied by a reduction in Q_{SH} and a negligible precipitation response. We believe that the precipitation response in this case is negligible because the perturbation is weak. To demonstrate it, we have run the model again with only the European plume but with 10 times larger AOD. Under this larger perturbation we do get a reduction in precipitation over Europe as predicted by the idealized perturbation simulation (Fig. S5, SI). However, the fact that we do not detect any significant reduction in precipitation over Europe in our simulations suggest that the magnitude of a realistic perturbation is not sufficient to cause a reduction in precipitation that could be observed.

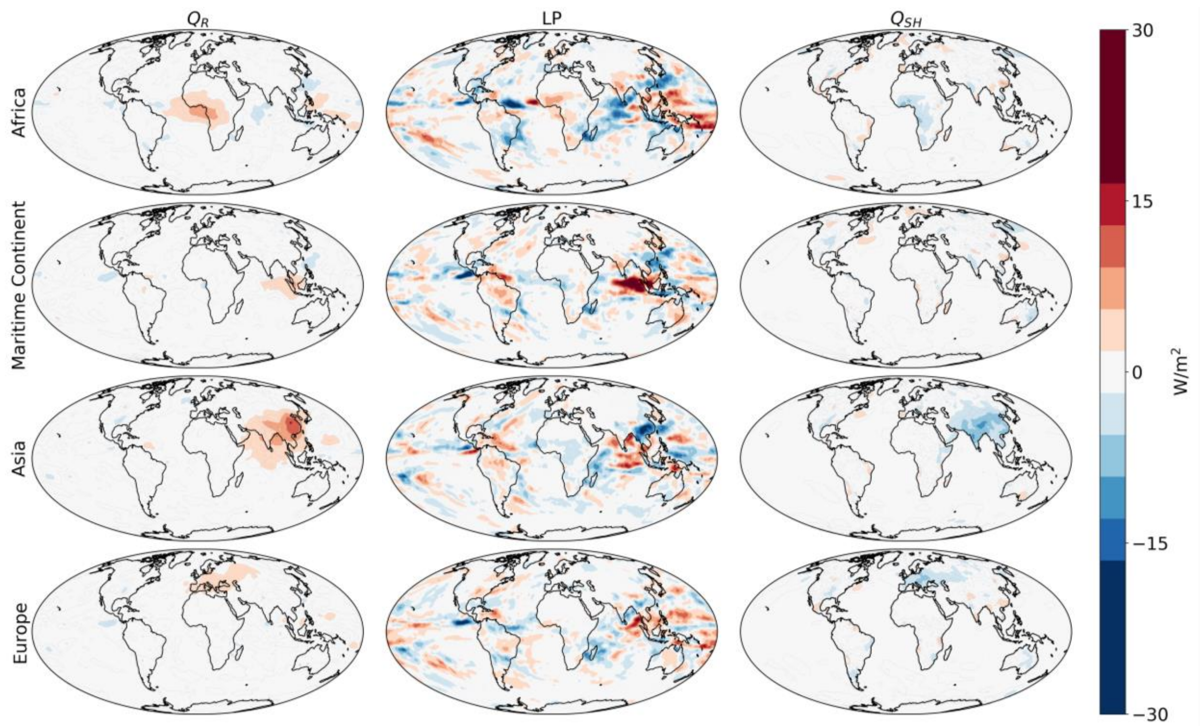

Figure 13. The atmospheric radiative heating (Q_R) perturbation (each simulation minus the reference simulation – left column), the precipitation latent heating change (middle column), and the sensible heat flux

(Q_{SH}) change (right column) in AMIP ICON simulations forced by individual aerosol plumes (based on Stevens et al., 2017). The individual plumes considered here are as listed in Table 1.

Examining regional precipitation response to local aerosol perturbation for different locations (Fig. 13) reduces the role of teleconnections. Namely, aerosol perturbation at a given location could affect precipitation at other locations as well due to changes in the large-scale dynamics and thermodynamics of the atmosphere (Allen et al., 2015; Chemke & Dagan, 2018; Dagan & Chemke, 2016; Rotstayn & Lohmann, 2002; Voigt et al., 2017; Wang, 2015). For including these effects and accounting for the global aerosol distribution we run the model with the full default MACv2-SP setup (Stevens et al., 2017), which includes, on top of the 6 aerosol plumes listed in Table 1, plumes over south and north America and over Australia. Figure 14 presents the precipitation response in this simulation. It demonstrates many similar features as in the individual plume experiments above, as well as in the idealized perturbation simulations. For example, it demonstrates an increase in precipitation over the tropical Indian ocean, a region forced by both the “Maritime Continent” plume and the south part of the “South Asia” plume. We also note a decrease in precipitation over east Asia land and the adjacent ocean, as in the Asian plume simulation. Figure 14 also shows an increase in precipitation over the east-tropical Atlantic Ocean (although less so over land), and a decrease in precipitation in the west-tropical Atlantic, a similar response as in the African plume simulation. However, the precipitation response appears to be noisy and it is not clear if it is statistically significant. In order to examine the robustness of the response presented in Fig. 14, we run the model with different magnitudes of AOD with the Full plume geographical distribution (increasing the AOD at the centre of each plume by 2, 5 and 10 times – Fig. 15). In addition, in figure 15 the locations in which the precipitation change is statistically significant (p-value < 0.05 according to a t-test) are marked. Indeed, Fig. 15 demonstrates that forcing the model with the default MACv2-SP setup (Full plume), for 30 years, generates fast precipitation changes, which are generally not statistically significant (even though its spatial structure is generally consistent with our physical understanding based on the idealized experiments).

Since the Full plume experiment demonstrates precipitation changes which are generally in agreement with the idealized perturbation and the single plume experiments, we believe that the fact that it is not statistically significant is a matter of signal-to-noise ratio (the response is not significant compared to the natural variability). This is demonstrated also by the simulations in which the AOD is increased (increasing the signal-to-noise ratio). The spatial correlation of the precipitation response is relatively high between the higher AOD simulations and the Full plume simulation (0.71, 0.66 and 0.55 for the 2, 5 and 10 times AOD simulations) indicating a similar spatial structure. However, the precipitation response (with the similar spatial structure) becomes more statistically significant as the AOD increases. This suggests that the response seen in the Full plume simulation is mostly due to a robust physical driver, but is not strong enough to emerge from the natural variability (over 30 years period with a prescribed SST). These results suggest that it will probably be hard to detect from observations the aerosol-radiation effect on precipitation over the last few decades (although the slow response might be more important over this time-period and is not accounted here). We note that running the model for longer period than 30 years might increase the signal-to-noise ratio, however, 30 years is already quite long period for examining the fast precipitation response as changes in SST could become important on that time-scales (Scannell et al., 2019).

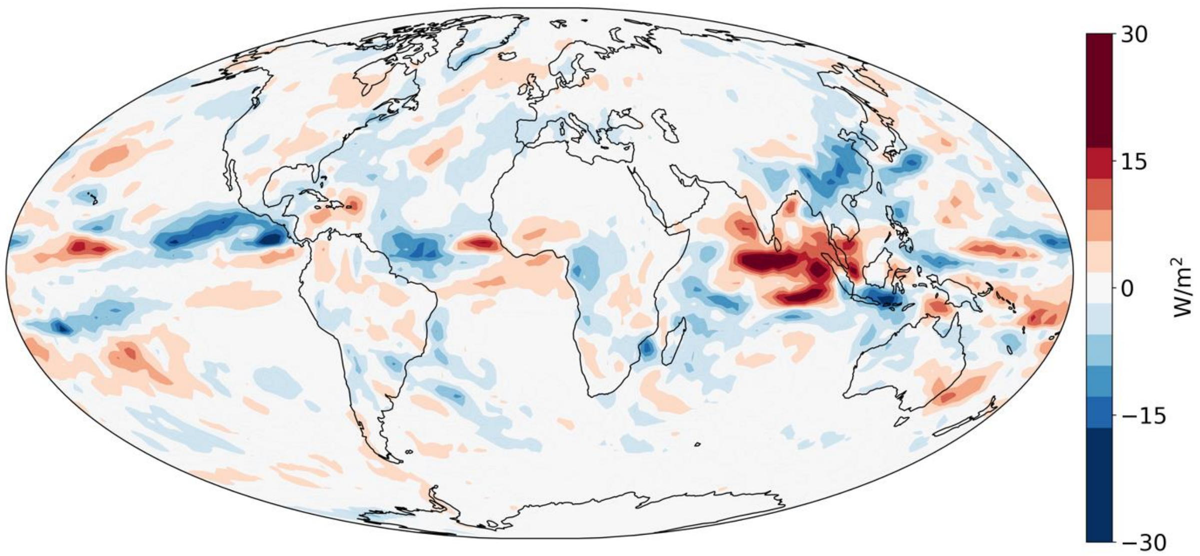

Figure 14. The precipitation latent heating change (compared to the reference simulation), in the AMIP ICON simulations forced by the full global distribution of aerosols (Full plume - based on Stevens et al., 2017).

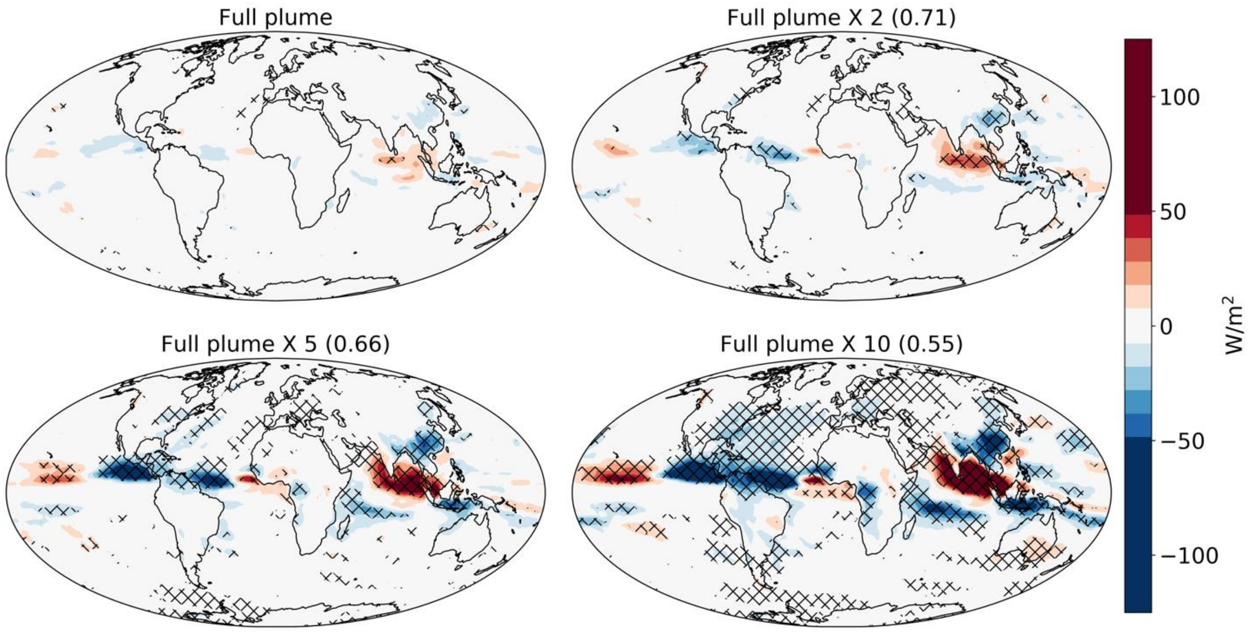

Figure 15. The precipitation latent heating change (compared to the reference simulation), in the AMIP ICON simulations forced by the full global distribution of aerosols for a few levels of AOD compared to the Full plume simulation (indicated in the title of each subplot). The spatial correlation of each simulation with the Full plume simulation is indicated in the parenthesis. Locations in which the precipitation change is statistically significant (p-value < 0.05 according to a t-test) are marked with crosses. Please note the different colour-bar as compared to Fig. 14. Figure S6, SI presents the relative precipitation change in these simulations.

Summary

Precipitation changes due to anthropogenic activity are hard to predict despite their importance for society (Allan et al., 2020; Dagan et al., 2019b; Knutti & Sedláček, 2013; Myhre et al., 2017). One anthropogenic driver for precipitation changes are aerosols, which can affect the amount of precipitation through interacting with clouds or with radiation. In this study, we examine fast precipitation changes (not mediated by changes in SST) due to aerosol-radiation interaction using a global model with idealised aerosol perturbations of different levels of complexities. Specifically, we expand the analysis of a previous study (Dagan et al., 2019a), which demonstrated a contrasting precipitation response in the tropics and extra-tropics based on aqua-planet simulations. The goals of the current study are three-fold, however, all related to the geographical location of the aerosol perturbation: 1) to identify the latitude in which a transition between a positive aerosol-driven precipitation response to a negative precipitation response occurs, 2) to examine the effect of land on the precipitation response, and 3) to examine the main conclusions under a more realistic aerosol perturbation in terms of magnitude and spatial structure. In this study we focus on the fast precipitation response (Bony et al., 2013; Myhre et al., 2018; Richardson et al., 2018) and the related physical mechanisms. In a future study we will examine the same trends in simulations with interactive SST, looking on the slow response.

Using idealized aqua-plant simulations with a stepwise increase in the aerosol plume latitude we show that the transition between an increase and a decrease in precipitation occurs at relatively low latitudes of ~10°. Equatorward of ~10°, the Coriolis effect is negligibly low, enabling a direct thermally-driven circulation to form as a response of aerosol diabatic-heating (Dagan et al., 2019a; Roeckner et al., 2006). Poleward of ~10° the Coriolis force is already sufficient to prevent the direct thermally-driven circulation and a geostrophic adjustment of the flow confines the heating perturbations. Hence, the local precipitation is reduced to maintain energy balance. We note the similarity with tropical cyclone genesis (Gray, 1975), which requires a sufficient Coriolis force to form cyclonic-circulation and to prevent the air from converging into the centre. Hence, tropical cyclones do not form within a few degrees away of the equator.

Next, we examine the effect of land using AMIP type of simulations with idealized aerosol perturbation (large magnitude and idealized spatial structure). These results demonstrate that, in the case of absorbing aerosols, the effect of land is to reduce both the positive precipitation response in the tropics and the negative response in the extra-tropics due to the reduction of the surface sensible heat flux. This reduction in sensible heat flux over land counteracts the diabatic-heating caused by absorbing aerosols and therefore reduces the effect as compared to over the ocean. In the case of scattering aerosols, surface cooling leads to an increase in surface pressure in the extra-tropics and corresponding anti-cyclonic circulation around the plume centre. This anti-cyclonic circulation drives subsidence and a reduction in cloudiness and precipitation. In the tropics, the surface pressure is less effected, but the reduction in surface shortwave radiation (due to scattering aerosols) drives a reduction in precipitation.

The fast precipitation response is also examined under more realistic aerosol perturbations (in terms of magnitude and spatial extent). This demonstrates that many of the features seen in the idealized simulations, as well as the underlying physical mechanisms, can explain the fast precipitation response under more realistic conditions. For example, we show that the absorbing aerosol perturbation near the equator (over Africa and Maritime Continent region) generates an increase in precipitation mostly over the ocean and less so over land (due to the role of the sensible heat flux). We also show that in the case of an aerosol perturbation over Asia, which extends all the way from the deep-tropics to the extra-tropics, the precipitation response is positive near the equator over the ocean and negative over land outside the deep-tropics. In the case of the realistic magnitude perturbation over Europe, we show that no precipitation response is seen and we demonstrate that this is because of a small perturbation (relatively low AOD with relatively high SSA). Forcing the model with a stronger perturbation (increasing the AOD over Europe by 10 times) generate a local reduction in precipitation, as predicted by the idealized simulations.

In the last part of this paper we force the model with the entire global distribution of aerosols, which includes changes in the large-scale circulation as well as teleconnections (Allen et al., 2015; Chemke & Dagan, 2018; Rotstayn & Lohmann, 2002; Voigt et al., 2017; Wang, 2015)) in addition to the local response due to changes in the energy budget. This demonstrates that many of the precipitation change features mentioned above are still relevant when the global aerosol distribution is included. However, the precipitation changes are shown to be statistically non-significant (for 30 years of simulations with a prescribed SST). We show that the fact that the precipitation changes are not statistically significant is not because it is inconsistent with our physical understanding of the system but because of a low signal-to-noise ratio. This is demonstrated through simulations in which the magnitude of the perturbation (AOD) is increased continually up to 10 times the default set-up, which is based on observations (Stevens et al., 2017). The precipitation changes under stronger perturbations have a similar (although not identical) spatial structure and are shown to be more statistically significant. These results suggest that the fast precipitation response to aerosol-radiative effects would be hard to observe in nature on decadal time-scales.

Data availability

The data presented in this manuscript will become available via Zenodo before the manuscript is published.

Acknowledgments

This research was supported by the European Research Council (ERC) project constRaining the EffeCts of Aerosols on Precipitation (RECAP) under the European Union's Horizon 2020 research and innovation programme with grant agreement No 724602. The simulations were performed using the ARCHER UK National Supercomputing Service. DWP receives funding from the European Union's Horizon 2020 research and innovation programme iMIRACLI under

Marie Skłodowska-Curie grant agreement No 860100. DWP also gratefully acknowledges funding from the NERC ACRUISE project NE/S005390/1.

References

Allan, R. P., Barlow, M., Byrne, M. P., Cherchi, A., Douville, H., Fowler, H. J., et al. (2020). Advances in understanding large-scale responses of the water cycle to climate change. *Annals of the New York Academy of Sciences*.

Allen, R. J., Evan, A. T., & Booth, B. B. (2015). Interhemispheric aerosol radiative forcing and tropical precipitation shifts during the late twentieth century. *Journal of climate, 28*(20), 8219-8246.

Allen, R. J., & Sherwood, S. C. (2011). The impact of natural versus anthropogenic aerosols on atmospheric circulation in the Community Atmosphere Model. *Climate Dynamics, 36*(9-10), 1959-1978.

Bony, S., Bellon, G., Klocke, D., Sherwood, S., Fermepin, S., & Denvil, S. (2013). Robust direct effect of carbon dioxide on tropical circulation and regional precipitation. *Nature Geoscience, 6*(6), 447.

Chemke, R., & Dagan, G. (2018). The Effects of the Spatial Distribution of Direct Anthropogenic Aerosols Radiative Forcing on Atmospheric Circulation. *Journal of climate, 31*(17), 7129-7145.

Crueger, T., Giorgetta, M. A., Brokopf, R., Esch, M., Fiedler, S., Hohenegger, C., et al. (2018). ICON-A: the atmospheric component of the ICON Earth System Model. Part II: Model evaluation. *Journal of Advances in Modeling Earth Systems, 10*, 1638-1662.

Dagan, G., & Chemke, R. (2016). The effect of subtropical aerosol loading on equatorial precipitation. *Geophysical research letters, 43*(20).

Dagan, G., Christensen, M., Stier, P., Seifert, A., Klocke, D., & Cioni, G. (2020). Atmospheric energy budget response to idealized aerosol perturbation in tropical cloud systems. *Atmospheric Chemistry and Physics, 20*(7).

Dagan, G., Stier, P., & Watson-Parris, D. (2019a). Contrasting response of precipitation to aerosol perturbation in the tropics and extra-tropics explained by energy budget considerations. *Geophysical research letters*.

Dagan, G., Stier, P., & Watson-Parris, D. (2019b). Analysis of the atmospheric water budget for elucidating the spatial scale of precipitation changes under climate change. *Geophysical research letters*.

Gates, W. L. (1992). AN AMS CONTINUING SERIES: GLOBAL CHANGE--AMIP: The Atmospheric Model Intercomparison Project. *Bulletin of the American Meteorological Society, 73*(12), 1962-1970.

Gill, A. E. (1980). Some simple solutions for heat-induced tropical circulation. *Quarterly Journal of the Royal Meteorological Society, 106*(449), 447-462.

Giorgetta, M. A., Brokopf, R., Crueger, T., Esch, M., Fiedler, S., Helmert, J., et al. (2018). ICON-A, the atmosphere component of the ICON Earth System Model. Part I: Model Description. *Journal of Advances in Modeling Earth Systems*.

Gray, W. M. (1975). Tropical cyclone genesis. *Atmospheric science paper; no. 234*.

Hodnebrog, O., Myhre, G., Forster, P. M., Sillmann, J., & Samset, B. H. (2016). Local biomass burning is a dominant cause of the observed precipitation reduction in southern Africa. *Nat Commun, 7*. Article. http://dx.doi.org/10.1038/ncomms11236

Jakob, C., Singh, M., & Jungandreas, L. (2019). Radiative Convective Equilibrium and Organized Convection: An Observational Perspective. *Journal of Geophysical Research: Atmospheres, 124*(10), 5418-5430.

Khain, A. P. (2009). Notes on state-of-the-art investigations of aerosol effects on precipitation: a critical review. *Environmental Research Letters, 4*(1), 015004 (015020 pp.)-015004 (015020 pp.). <Go to ISI>://INSPEC:10995649

Kinne, S., O'Donnel, D., Stier, P., Kloster, S., Zhang, K., Schmidt, H., et al. (2013). MAC-v1: A new global aerosol climatology for climate studies. *Journal of Advances in Modeling Earth Systems, 5*(4), 704-740.

Knutti, R., & Sedláček, J. (2013). Robustness and uncertainties in the new CMIP5 climate model projections. *Nature Climate Change, 3*(4), 369.

Levin, Z., & Cotton, W. R. (2009). *Aerosol pollution impact on precipitation: A scientific review* (Z. Levin & W. R. Cotton Eds.): Springer.

Liu, L., Shawki, D., Voulgarakis, A., Kasoar, M., Samset, B., Myhre, G., et al. (2018). A PDRMIP Multimodel Study on the impacts of regional aerosol forcings on global and regional precipitation. *Journal of climate, 31*(11), 4429-4447.

Matsuno, T. (1966). Quasi-geostrophic motions in the equatorial area. *Journal of the Meteorological Society of Japan. Ser. II, 44*(1), 25-43.

Ming, Y., Ramaswamy, V., & Chen, G. (2011). A model investigation of aerosol-induced changes in boreal winter extratropical circulation. *Journal of climate, 24*(23), 6077-6091.

Muller, C., & O’Gorman, P. (2011). An energetic perspective on the regional response of precipitation to climate change. *Nature Climate Change, 1*(5), 266.

Myhre, G., Forster, P., Samset, B., Hodnebrog, Ø., Sillmann, J., Aalbergsjø, S., et al. (2017). PDRMIP: a precipitation driver and response model intercomparison project—protocol and preliminary results. *Bulletin of the American Meteorological Society, 98*(6), 1185-1198.

Myhre, G., Kramer, R., Smith, C., Hodnebrog, Ø., Forster, P., Soden, B., et al. (2018). Quantifying the importance of rapid adjustments for global precipitation changes. *Geophysical research letters, 45*(20), 11,399-311,405.

Ramanathan, V., Crutzen, P., Kiehl, J., & Rosenfeld, D. (2001). Aerosols, climate, and the hydrological cycle. *science, 294*(5549), 2119-2124.

Richardson, T., Forster, P., Andrews, T., Boucher, O., Faluvegi, G., Fläschner, D., et al. (2018). Drivers of precipitation change: An energetic understanding. *Journal of climate, 31*(23), 9641-9657.

Roeckner, E., Stier, P., Feichter, J., Kloster, S., Esch, M., & Fischer-Bruns, I. (2006). Impact of carbonaceous aerosol emissions on regional climate change. *Climate Dynamics, 27*(6), 553-571.

Rotstayn, L. D., & Lohmann, U. (2002). Tropical rainfall trends and the indirect aerosol effect. *Journal of climate, 15*(15), 2103-2116. <Go to ISI>://WOS:000177007200007

Samset, B., Myhre, G., Forster, P., Hodnebrog, Ø., Andrews, T., Faluvegi, G., et al. (2016). Fast and slow precipitation responses to individual climate forcers: A PDRMIP multimodel study. *Geophysical research letters, 43*(6), 2782-2791.

Scannell, C., Booth, B. B., Dunstone, N. J., Rowell, D. P., Bernie, D. J., Kasoar, M., et al. (2019). The Influence of Remote Aerosol Forcing from Industrialized Economies on the Future Evolution of East and West African Rainfall. *Journal of climate, 32*(23), 8335-8354.

Sobel, A. H., Nilsson, J., & Polvani, L. M. (2001). The weak temperature gradient approximation and balanced tropical moisture waves. *Journal of the Atmospheric Sciences, 58*(23), 3650-3665.

Stevens, B., Fiedler, S., Kinne, S., Peters, K., Rast, S., Müsse, J., et al. (2017). MACv2-SP: a parameterization of anthropogenic aerosol optical properties and an associated Twomey effect for use in CMIP6. *Geoscientific Model Development, 10,* 433-452.

Stuecker, M. F., Timmermann, A., Jin, F.-F., Proistosescu, C., Kang, S. M., Kim, D., et al. (2020). Strong remote control of future equatorial warming by off-equatorial forcing. *Nature Climate Change*, 1-6.

Voigt, A., Pincus, R., Stevens, B., Bony, S., Boucher, O., Bellouin, N., et al. (2017). Fast and slow shifts of the zonal-mean intertropical convergence zone in response to an idealized anthropogenic aerosol. *Journal of Advances in Modeling Earth Systems, 9*(2), 870-892.

Wang, C. (2015). Anthropogenic aerosols and the distribution of past large-scale precipitation change. *Geophysical research letters*.

Zängl, G., Reinert, D., Rípodas, P., & Baldauf, M. (2015). The ICON (ICOsahedral Non-hydrostatic) modelling framework of DWD and MPI-M: Description of the non-hydrostatic dynamical core. *Quarterly Journal of the Royal Meteorological Society, 141*(687), 563-579.

Zhao, A. D., Stevenson, D. S., & Bollasina, M. A. (2019). The role of anthropogenic aerosols in future precipitation extremes over the Asian Monsoon Region. *Climate Dynamics, 52*(9-10), 6257-6278.